




Article

Activated Carbon Prepared from Waste Coffee Grounds: Characterization and Adsorption Properties of Dyes

Feryelle Aouay ^{1,2} , Afef Attia ¹ , Lasâad Dammak ³ , Raja Ben Amar ^{1,*} and Andre Deratani ^{2,*}

¹ Research Unit “Advanced Technologies for Environment and Smart Cities”, Faculty of Sciences, University of Sfax, 3000 Sfax, Tunisia; afef.attia@fss.usf.tn (A.A.)

² Institut Européen des Membranes, IEM UMR-5635, CNRS, ENSCM, University Montpellier, Place Eugène Bataillon, 34095 Montpellier, France

³ Institut de Chimie et des Matériaux Paris Est, ICMPE UMR-CNRS 7182-UPEC, Université Paris Est Creteil 2 rue Henri Dunant, 94320 Thiais, France; dammak@u-pec.fr

* Correspondence: raja.benamar@fss.usf.tn (R.B.A.); andre.deratani@umontpellier.fr (A.D.)

Abstract: Spent coffee grounds (SCGs) have great potential as a useful, value-added biological material. In this context, activated carbon (AC) was prepared from SCGs by an activation process using H_3PO_4 at 600 °C in the air and used as an adsorbent for the azo dye AO7, a model molecule for dye colorants found in textile industry effluents. X-ray diffraction, SEM and BET revealed that the AC was predominantly amorphous, consisting of a powder of 20–100 μm particles with mesopores averaging 5.5 nm in pore size. Adsorption kinetics followed a pseudo-second-order law, while the Langmuir model best fitted the experimental isotherm data (maximum capacity of 119.5 mg AO7 per AC g). The thermodynamic parameters revealed that adsorption was endothermic and spontaneous. All the characterizations indicated that adsorption occurred by physisorption via mainly π – π interactions. The best experimental removal efficiency optimized by means of a Box–Behnken design and response surface methodology was 98% for an initial AO7 concentration of 20 $\text{mg}\cdot\text{L}^{-1}$ at pH 7.5 with a dose of 0.285 $\text{g}\cdot\text{L}^{-1}$ of AC and a contact time of 40 min. These results clearly show that activated carbon prepared from SCGs can be a useful material for efficiently removing organic matter from aqueous solutions.

Keywords: dye removal; AO7; activated carbon; spent coffee grounds; adsorption process; experimental design methodology; optimization



Citation: Aouay, F.; Attia, A.; Dammak, L.; Ben Amar, R.; Deratani, A. Activated Carbon Prepared from Waste Coffee Grounds: Characterization and Adsorption Properties of Dyes. *Materials* **2024**, *17*, 3078. <https://doi.org/10.3390/ma17133078>

Academic Editor: Agata Jakóbik-Kolon

Received: 29 April 2024

Revised: 12 June 2024

Accepted: 18 June 2024

Published: 22 June 2024



Copyright: © 2024 by the authors. Licensee MDPI, Basel, Switzerland. This article is an open access article distributed under the terms and conditions of the Creative Commons Attribution (CC BY) license (<https://creativecommons.org/licenses/by/4.0/>).

1. Introduction

Water is an essential resource which integrity is often compromised by the discharge of industrial waste containing harmful substances into natural environments [1]. A striking example of this challenge is the treatment of contaminated industrial wastewater, particularly from the textile industry, one of the biggest water consumers [2]. This industry generates a large volume of waste loaded with dyes and chemicals, posing a threat to human health and the environment [3]. It is responsible for the largest amount of wastewater compared to other industries, at over 56% [4,5]. Recent estimates have indicated an annual consumption of more than 10,000 tons of over 100,000 commercial dyes [6–9]. Approximately 10–15% of the dye is lost during the dyeing process, and around 20% of the lost dye ends up in wastewater [10,11], with a concentration of up to 1 $\text{mg}\cdot\text{L}^{-1}$ [12,13]. Synthetic dyes, especially azo dyes, are of particular concern because of their carcinogenic, mutagenic and teratogenic properties, as well as the high chemical and biological oxygen demand required for their degradation [14,15]. Acid Orange 7 (AO7), an azo dye widely used as a model molecule, exemplifies these challenges. Despite its water solubility and stability, AO7 can cause methemoglobinemia upon human exposure, resulting in symptoms such as cyanosis and weakness [15–17].

Azo dyes, characterized by an azo chromophore group ($-\text{N}=\text{N}-$) and an electron-receiving sulfonate group ($-\text{SO}_3^-$), are difficult to degrade by conventional processing

methods [18–20]. In fact, textile dyes are not easily biodegradable, requiring the development of specific microbial strains and immobilized enzymes [21]. Another approach to decontaminating water polluted by textile dyes is the use of physicochemical techniques, including electrochemical oxidation [22], coagulation-flocculation [23], filtration [24,25] and photodegradation [26]. However, these methods often have drawbacks, such as high costs and the production of toxic by-products. Adsorption appears to be a promising alternative approach due to its cost-effectiveness and its ability to remove contaminants without introducing additional toxicity. A number of different approaches have been developed [27–29]. Activated carbon (AC) is emerging as an adsorbent of choice, especially when derived from natural biopolymers or waste products, offering a sustainable and cost-effective solution for water purification [8]. The production of AC from inexpensive feedstocks available in large quantities makes it possible to envisage an easily scalable adsorption process [30]. In this work, spent coffee grounds (SCGs) were chosen as a precursor to produce AC [31,32].

Coffee is one of the world’s most popular beverages. Every year, more than five million tons of coffee are produced worldwide (International Coffee Organization, London, UK, 2022). Generally, SCGs are disposed of by composting, incineration or landfill. It has been reported that these methods can have a negative impact on the environment, releasing contaminating residues of tannin, caffeine and polyphenols [33]. Other ways of valorizing SCGs have been proposed, such as converting them into biofuel, biodiesel, bioethanol or biomaterials [34] and producing biochar and AC [35–37]. These routes can help reinforce the circular economy approach by enabling continuous processes that reduce the accumulation of waste by transforming it into useful, value-added materials while promoting more environmentally friendly models [38,39].

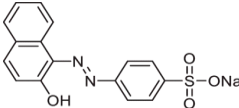
This study examined the removal of AO7, as a model molecule for azo dye used in textile industry, by adsorption onto AC produced from SCGs. The physicochemical properties of the AC produced were investigated using techniques such as TGA-DTG, XRD, FT-IR and SEM. With a view toward optimizing the process, studies including adsorption kinetics and isotherms, as well as thermodynamic characteristics, were carried out to understand how certain experimental parameters such as the dye concentration/adsorbent quantity ratio and contact time can affect the adsorption operation. A statistical analysis was then applied to assess the weight of each of the experimental parameters. The response surface methodology (RSM) model was used to analyze the interactions among the parameters studied in order to gain a better insight into their combined effects. This method has the advantage of evaluating several parameters at once, which reduces the number of experiments required and saves time compared to the traditional method of examining one factor at a time [40,41]. In addition, the efficiency of experimental systems can be effectively evaluated and process variability minimized.

2. Materials and Methods

2.1. Chemicals

The SCGs used in the present study were collected from local coffee shops and served as a low-cost precursor for AC. Phosphoric acid (H_3PO_4 , 50%) was used as a chemical activating agent in the preparation of AC. The azo dye AO7 (analytical grade $\geq 85\%$), which characteristics are given in Table 1, was supplied by Sigma-Aldrich (St. Louis, MO, USA). All aqueous solutions were prepared with deionized water and pH-adjusted with sodium hydroxide (NaOH, 0.2 M) and hydrochloric acid (HCl, 0.2 M).

Table 1. Main characteristics of AO7.

Chemical Structure	Molecular Formula	Molecular Weight (g·mol ⁻¹)	Solubility in Water (g·L ⁻¹)	Melting Point (°C)	λ Max (nm)
	$C_{16}H_{11}N_2SO_4Na$	350.32	116	164	483

2.2. Activated Carbon Preparation

Two batches of SCG-based AC were prepared according to the following procedure, adapted from [42]. Typically, SCGs (30 g) were washed with deionized water, then dried in an oven at 60 °C. The resulting dried SCGs were immersed in a 50% solution of H₃PO₄ in a weight ratio of 1:3 (SCG:H₃PO₄) and stirred at 80 °C for 3 h. Slow pyrolysis was then carried out at 600 °C for 2 h in a muffle furnace in the air. The resulting AC was washed with deionized water to a neutral pH and then finally dried in an electric oven at 105 °C for 24 h.

2.3. Characterization of AC

The produced AC was characterized using FTIR (Spectrum 100, Perkin Elmer, Waltham, MA, USA) and SEM (Quanta-250, Thermo Fisher Scientific, Waltham, MA, USA) at an accelerating voltage of 20 kV to identify the surface functional groups and morphologies, respectively. The specific surface area, total pore volume and pore diameter were measured using the Brunauer, Emmett and Teller (BET) method (ASAP 2020, Micromeritics, Norcross, GA, USA). The crystalline structure was determined by X-ray diffraction (XRD 6000, Shimadzu, Kyoto, Japan) using Cu K α 1 ($\lambda = 1.5046 \text{ \AA}$) with an X-ray source through the 2θ range from 4° to 80°. Thermogravimetric analysis (TGA; Labsys evo1150, Setaram, Caluire-et-Cuire, France) was carried out to determine the thermal stability.

The zero charge point is the pH at which the AC surface becomes neutral. This value (pH_{PZC}) was determined using the following procedure: 50 mL of NaCl solution (0.01 M) with pH values ranging from 1 to 10 was prepared by adding NaOH solution (0.2 M) and HCl solution (0.2 M), then 100 mg of AC was added to each solution and left to stir for 48 h at room temperature. The final pH after 48 h was recorded to calculate the pH change. The pH_{PZC} point was identified at the intersection of the curve (final pH—initial pH) and the straight line (final pH = initial pH) using a graphical representation of the data.

2.4. Batch Adsorption Studies

A stock solution was prepared at 0.1 g·L⁻¹ from AO7 as purchased. The concentrations required for the adsorption experiments were obtained by dilution with deionized water. The desired amount of AC, depending on the experimental conditions chosen, was added to the 100 mL dye solution under magnetic stirring (500 rpm) at room temperature (about 25 °C). The pH was 7.5 and remained unchanged during the adsorption experiments. Once the adsorption process was complete, the solution mixture was passed through a 0.45 μm syringe filter. The filtrate obtained was then analyzed using a UV–Visible spectrophotometer at a wavelength of 483 nm to determine the percentage of dye removal according to the calibration curve. The dye adsorption capacity and removal efficiency of the adsorbent were quantified using Equations (1) and (2), respectively.

$$q_t = \frac{C_0 - C_t}{M} \cdot V \quad (1)$$

$$R = \frac{C_0 - C_t}{C_0} \cdot 100 \quad (2)$$

where q_t (mg·g⁻¹) is the adsorption capacity at time t , R the AO7 dye removal efficiency, C_0 the initial dye concentration, C_t (mg·L⁻¹) the dye concentration at time t , V (mL) the solution volume and M (g), the mass of the AC adsorbent.

2.5. Adsorption Kinetics

The kinetics of the adsorption process were evaluated by varying the contact time between AO7 and AC. The experiment was carried out in a 200 mL suspension with a dye concentration of 30 mg·L⁻¹ and 0.6 g AC. The concentration of dye in the solution was determined every 10 min until equilibrium was reached, when its value remained constant. The data were then fitted to pseudo-first-order and pseudo-second-order models (equations presented in Table 2).

Table 2. Kinetic models.

Kinetic Model	Equation
Pseudo-first-order	$\log(q_e - q_t) = \log q_e - \frac{K_f \cdot t}{2303}$ (3)
Pseudo-second-order	$\frac{t}{q_t} = \frac{1}{K_s \cdot q_e^2} + \frac{t}{q_e}$ (4)

where q_t and q_e ($\text{mg} \cdot \text{g}^{-1}$) are the adsorption capacity at time t and equilibrium, respectively, and K_f and K_s are the pseudo-first-order (min^{-1}) and pseudo-second-order ($\text{g} (\text{mg} \cdot \text{min})^{-1}$) adsorption rate constants, respectively.

2.6. Adsorption Isotherms

Adsorption isotherm models can be used to highlight the interactions of AO7 molecules with adsorption sites on the AC surface. This experiment examined the correlation between the amount of dye adsorbed at equilibrium and the amount of sorbent used. For this study, the dye concentrations ranged from 10 to 90 $\text{mg} \cdot \text{L}^{-1}$, while the AC quantity and contact time were kept constant and equal to 0.3 $\text{g} \cdot \text{L}^{-1}$ and 60 min, respectively. Data adequacy and characterization of the adsorbent surfaces as heterogeneous or homogeneous were assessed using Langmuir and Freundlich isotherm models (linearized equations presented in Table 3).

Table 3. Isotherm models.

Isotherm Model	Equation
Langmuir	$\frac{C_e}{q_e} = \frac{1}{K_L \cdot q_{max}} + \frac{C_e}{q_{max}}$ (5)
Freundlich	$\log q_e = \log k_f + \frac{1}{n} \cdot \log C_e$ (6)

where q_{max} and q_e ($\text{mg} \cdot \text{g}^{-1}$) are the maximum monolayer adsorption capacity of the adsorbent and at equilibrium in Equations (5) and (6), respectively, C_e ($\text{mg} \cdot \text{L}^{-1}$) the equilibrium value of the initial concentration, K_L the Langmuir constant ($\text{mg} \cdot \text{L}^{-1}$) and K_f the Freundlich constant.

2.7. Adsorption Thermodynamics

Equilibrium adsorption isotherms were performed at three different temperatures (298, 321 and 339 K) to determine the thermodynamic parameters, such as enthalpy, entropy and Gibbs free energy, using Equations (7)–(9) presented in Table 4.

Table 4. Thermodynamic parameters.

Thermodynamic Parameters	Equation
Gibbs free energy	$K_c = K_L \cdot 1000 \cdot 55.51 \cdot Mw$ (7)
	$\Delta G^\circ = -RT \ln K_c$ (8)
Enthalpy	$\ln K_c = \left(\frac{\Delta S^\circ}{R} \right) - \left(\frac{\Delta H^\circ}{R} \right) \cdot \frac{1}{T}$ (9)
Entropy	

where K_c (dimensionless) is the equilibrium constant; K_L ($\text{L} \cdot \text{mg}^{-1}$) the Langmuir constant; 55.51 the number of moles of pure water per liter ($\text{mol} \cdot \text{L}^{-1}$); Mw ($\text{g} \cdot \text{mol}^{-1}$) the molecular weight of the dye; T ($^\circ\text{K}$) is the absolute temperature; R the ideal gas constant ($8.314 \text{ J} \cdot \text{mol}^{-1} \cdot \text{K}^{-1}$); and ΔG° ($\text{kJ} \cdot \text{mol}^{-1}$) is the Gibbs free energy change, ΔH° ($\text{kJ} \cdot \text{mol}^{-1}$) the enthalpy change and ΔS° ($\text{J} \cdot \text{mol}^{-1} \cdot \text{K}^{-1}$) the entropy change.

2.8. Optimization of AO7 Removal by AC Adsorption

A Box–Benken quadratic three-factor response RSM model was developed to determine the impact of three independent variables on AO7 dye removal: contact time (X_1), initial dye concentration (X_2) and adsorbent dose (X_3). This approach made it possible to optimize the response variable (Y) as a function of the input variables while reducing the amount of experimental work required for the adsorption studies. Design-Expert v12 software (Stat-Ease, Minneapolis, MI, USA) was applied to analyze the data using the RSM approach. In this study, the box in which the selected parameters were varied was 10–60 min for the contact time, 10–90 $\text{mg} \cdot \text{L}^{-1}$ for the initial dye concentration and 0.1–0.4 $\text{g} \cdot \text{L}^{-1}$ for the adsorbent dose. Fifteen experiments were designed to optimize the combination of input variables, with AO7 dye removal efficiency (%) used as the output response. To

assess the model fit, analysis of variance (ANOVA) was used. The results derived from the experimental design, structured in three levels, were fitted using a model designed to capture the desired response. A classical polynomial regression equation was used to express the predicted response (Y):

$$Y(\%) = a_0 + \sum a_i X_i + \sum \sum a_{ij} X_i X_j + \sum a_{ii} X_i^2, i \neq j \quad (10)$$

where the X_i is the input factors that can influence the response Y , n the number of variables, a_0 the constant intercept, a_i the linear and a_{ii} the quadratic coefficient (with $(i = 1, 2, \dots, n)$ and a_{ij} ($i = 1, 2, \dots, n - 1; j = 2, \dots, n$) the interaction coefficient between two input factors. The regression and RSM models were used to investigate the highest projected dye removal.

3. Results and Discussion

Two batches of AC were prepared. Very similar results were obtained in terms of material characterization and adsorption properties.

3.1. Characteristics of the Prepared Activated Carbon

3.1.1. Chemical Group Analysis

The raw SCG mixture and the AC produced were compared using the FTIR technique to highlight the change in characteristic functional groups during activation (Figure 1a,b). The following band assignments were made based on the data found in the literature [43–45]:

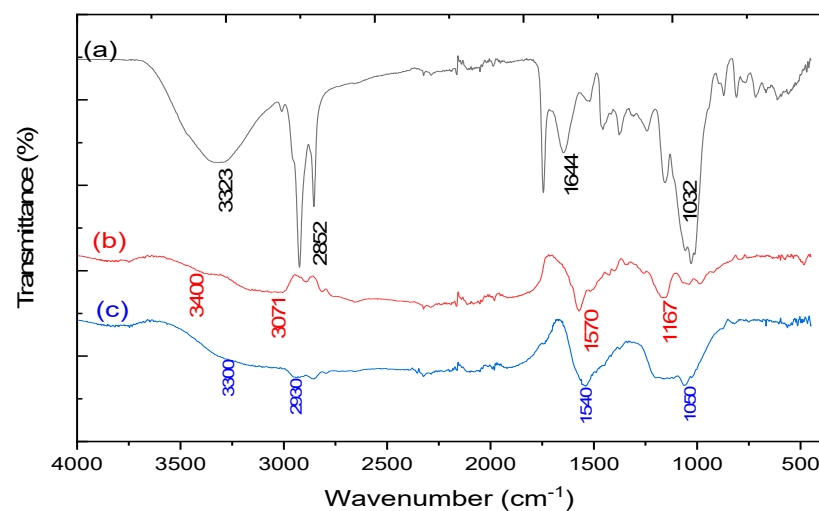


Figure 1. The FTIR spectrum for SCGs (a). AC before (b) and after dye adsorption (c).

- The presence in the SCG spectrum (Figure 1a) of a broad transmission band between 3200 and 3600 cm^{-1} was attributed to the O-H stretching vibrations in cellulose, hemicellulose and lignin molecules. This band almost disappeared in the AC spectrum (Figure 1b) due to dehydration caused by the combination of H_3PO_4 and heat action.
- The sharp bands at 2800–3000 cm^{-1} can be assigned to stretch vibrations of the C-H bond in the saturated hydrocarbons. These strong absorptions in the SCG spectrum have been assumed due to the presence of components other than cellulose, hemicellulose and lignin molecules [44]. These bands disappeared in the AC spectrum, probably indicating their decomposition during pyrolysis.
- The bands between 1650 and 1750 cm^{-1} characteristic of carbonyl groups in the SCG spectrum revealed the presence of lignin and the strong absorption observed in the 1000–1200 cm^{-1} region linked to C-O stretching vibrations of cellulose, hemicellulose and lignin.
- As expected, AC showed stronger absorption than the starting SCG material around 1600 cm^{-1} corresponding to the C=C vibrations in aromatic rings due to pyrolysis. On

the other hand, the broad band around 1200 cm^{-1} was attributed to P=O and P-O-C vibrations associated with H_3PO_4 activation.

Comparison of the AC spectra before and after dye adsorption (Figure 1b,c) revealed only slight changes due to a strong overlap of their respective characteristic bands. However, an increase in absorption in the $1500\text{--}1550\text{ cm}^{-1}$ range linked to the vibrations of azo groups (-N=N-) was observed, confirming the AO7 adsorption.

3.1.2. Structural Characterization

The X-ray diffraction was used to study the existence of crystalline structures and the amorphous nature within the AC matrix (Figure 2). The powder spectrum obtained revealed two diffraction peaks at about $2\theta = 24$ and 44° , as is usually observed for AC prepared from different sources, indicating that the activation process was successful [42,46–48]. The peaks observed are generally associated with the (002) and (100) reflection planes of graphite. However, as can be seen, the diffraction peaks are quite broad, suggesting that the structure of the prepared AC consisted of small crystalline phases dispersed in large disordered zones.

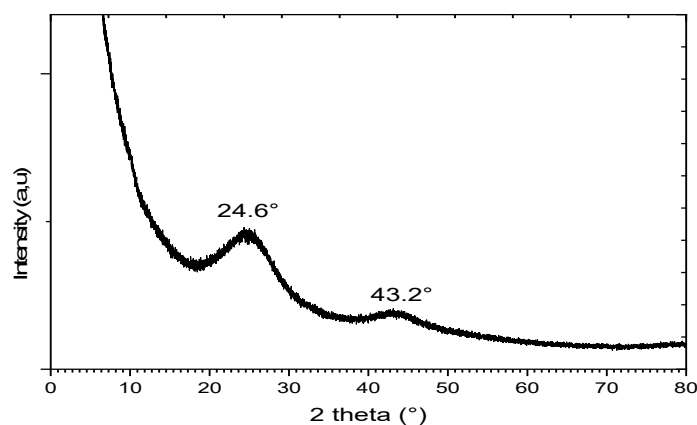


Figure 2. XRD pattern for the AC prepared from SCGs.

The amorphous structure of adsorbent is expected to create a favorable microenvironment for the adsorption of molecules in large quantities with a stronger bond. In contrast, crystalline structures have uniform shapes, making the adsorption ability difficult. The AC prepared from SCGs in this work presented a structure suitable for having good adsorption capability.

3.1.3. Morphological Analysis

SEM analysis provided useful information on the shape, size and structure of the AC powder particles (Figure 3). The irregular-shaped particles showed a polydisperse size distribution with dimensions ranging mainly from about 20 to $100\ \mu\text{m}$. In addition, SEM images enabled us to characterize the porous structure generated during the acid activation and pyrolysis processes. The outer surface of the particles had a macroporous morphology with cavity smaller than $20\ \mu\text{m}$. The enlargement in Figure 3 shows that interconnection by smaller pores in the cavities ensures the penetration and transfer of low-molecular-weight molecules from the surface to the inner microporosity of the adsorbent.

3.1.4. Textural Properties

Activated carbons are porous substances with a wide variety of pores ranging from macropores ($>50\text{ nm}$) to mesopores ($2\text{--}50\text{ nm}$) and occasionally a small number of micropores ($<2\text{ nm}$), depending on the activation process [29]. Gas adsorption—in particular, nitrogen adsorption at 77 K —is a commonly used method for studying the characteristics of porous activated carbons. Figure 4a,b show the hysteresis of the adsorption isotherm and the pore distribution deduced for the AC sample, respectively. The material mainly

exhibited a mesoporous structure according to IUPAC standards (Figure 4a; Type IV isotherm) [49], with a surface area and pore volume at 295 K of $29.38 \text{ m}^2 \cdot \text{g}$ and $0.067 \text{ cm}^3 \cdot \text{g}$, respectively (Table 5). These values are easily explained by the reduction in the surface area and total volume of AC pores due to pyrolysis, which leads to pore collapse in composite materials [50]. However, given the small molecular size of the dyes, and of AO7 in particular (Table 1), the mean pore size (D_m) of 5.5 nm appears large enough to allow internal mass transfer of these compounds within the AC porous structure.

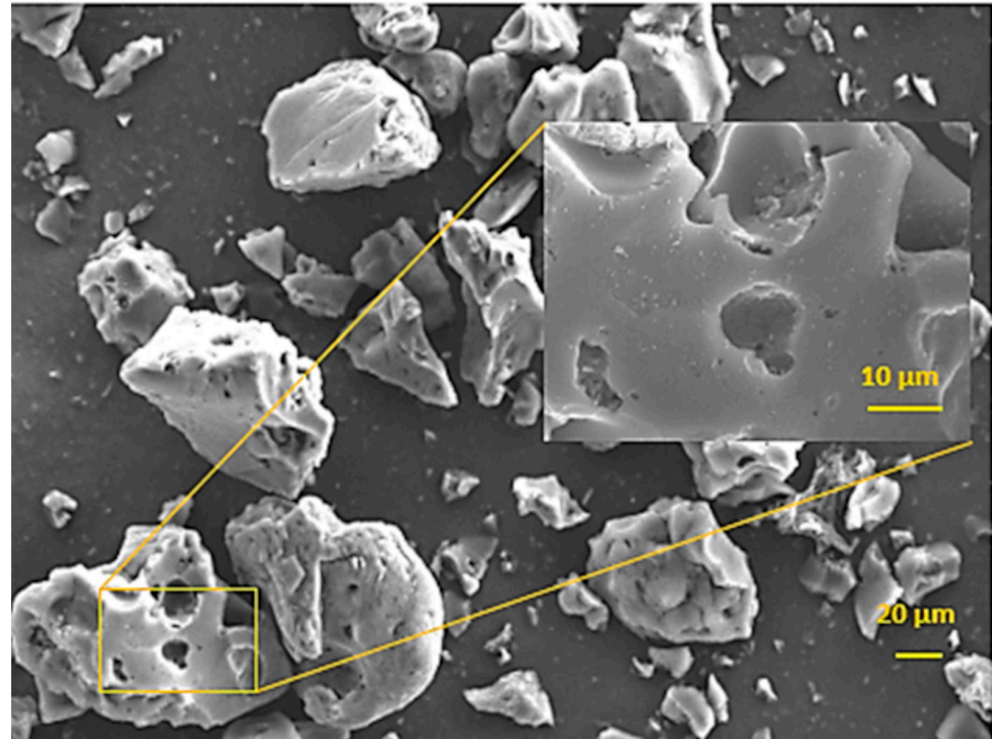


Figure 3. SEM surface image of AC prepared from SCGs.

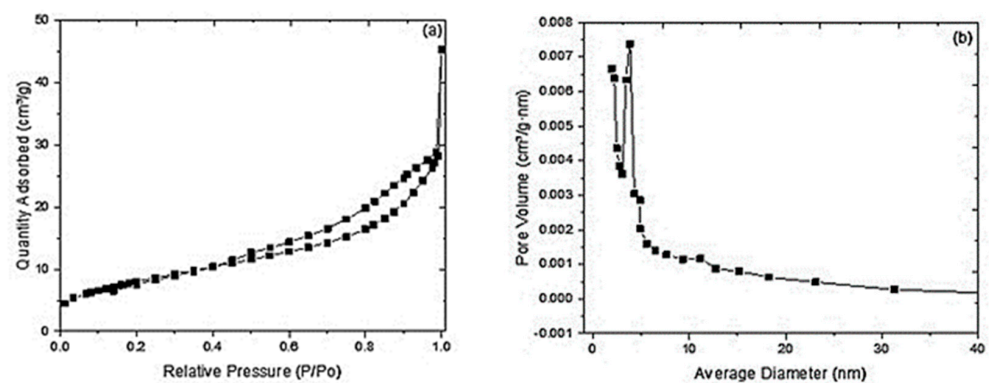


Figure 4. (a) N_2 adsorption/desorption isotherms. (b) Pore size distribution of AC.

Table 5. BET measurements of AC.

	S_{BET} ($\text{m}^2 \cdot \text{g}$)	V_{total} ($\text{cm}^3 \cdot \text{g}$)	D_m (nm)
AC (from SCG)	29.38	0.067	5.5

3.1.5. Thermal Stability

Figure 5 shows the variation in AC weight between 50 and 1100 °C using TGA. The thermogram obtained displays that a significant mass loss, equivalent to about 20%,

occurred from 50 °C to 150 °C. It mainly corresponded to the removal of moisture (DTG peak at 100 °C) and, possibly, of volatile compounds that accumulated within the porous structure of the material during its storage [51]. This result is indicative of the excellent adsorption properties of AC prepared in this work. Then, the curve shows a plateau up to 450 °C with no significant mass loss, revealing high thermal resistance and possible applications in this temperature range. After this second region, a gradual weight loss of about 30% is observed from 450 °C to 1100 °C. This mass decrease is due to decomposition of the oxygenated functions and partial degradation of the carbon skeleton [52,53].

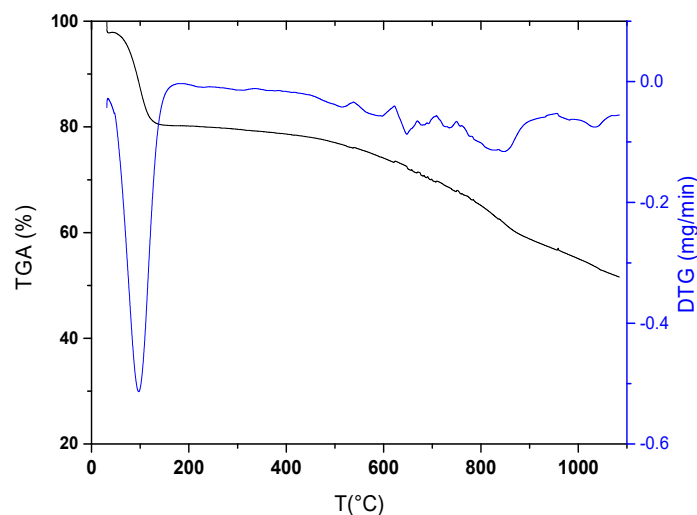


Figure 5. TGA and DTG curves of AC prepared from SCGs.

3.1.6. pH Determination of Zero Charge Point

The surface charge of an adsorbent as a function of pH is an important parameter for the adsorption process, as it depends on the chemical groups present on the surface. Figure 6 presents the shift in pH AC suspension compared to the corresponding blank solutions. The intersection of curves at pH 2.4 indicates when the net AC surface charge becomes neutral at this value (pH_{PZC}). This implies that, for pH above this, the number of negatively charged surface functions is higher than that of positively charged functions, mainly due to deprotonation of the carboxylic and phenolic groups [53].

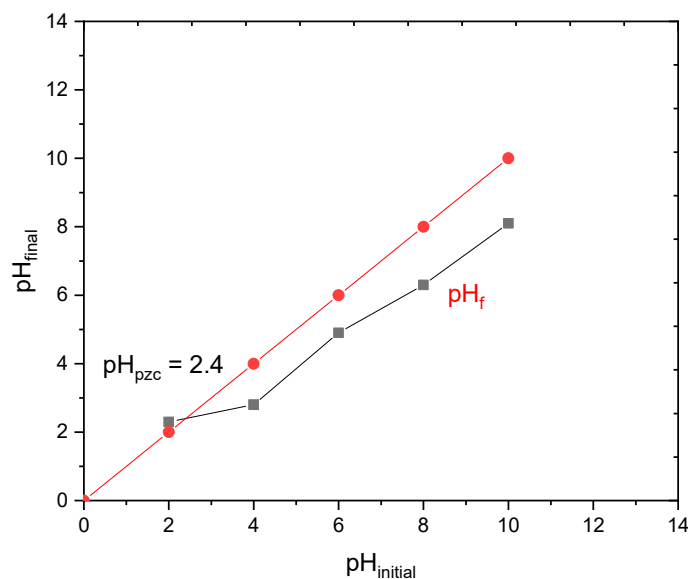


Figure 6. Determination of the point of zero charge pH.

3.2. Dye Adsorption Characterization

3.2.1. Adsorption Kinetics

Adsorption kinetics and analysis of the quantity adsorbed at equilibrium are the two key parameters for understanding and optimizing the adsorption process. The rate of removal of the AO7 dye from solution by AC was studied in order to establish the kinetic laws of adsorption. These experimental data were modeled in Figure 7 using two theoretical approaches: the pseudo-first-order (PFO) model and the pseudo-second-order (PSO) model (Table 2).

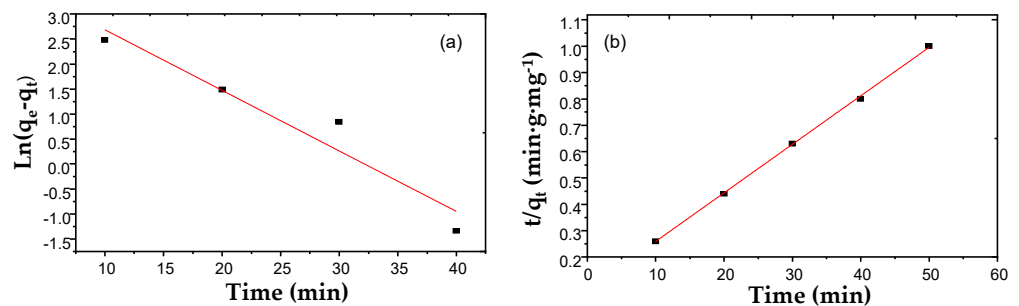


Figure 7. Kinetic plots and fitted kinetic model curve for AO7 adsorption on AC: (a) pseudo-first-order kinetic and (b) pseudo-second-order models.

The best fitting for each of the two Equations (3) and (4) were obtained using the coefficients listed in Table 6. It was found that experimental data fitted the PSO model (Figure 7b) much better than the PFO model (Figure 7a). The quantities of dye adsorbed on AC (q_{exp}) were almost identical to those calculated (R^2 values close to unity). These results confirm the relevance of the PSO model to describe the adsorption kinetics of the AO7 dye on the AC surface and agree fully with previously reported data for the adsorption of various dyes on activated carbon [29].

Table 6. Kinetic parameters for AO7 adsorption.

Pseudo-First-Order			Pseudo-Second-Order		
K_f (min ⁻¹)	q_e (mg·g ⁻¹)	R^2	K_s (mg·(g·min) ⁻¹)	q_e (mg·g ⁻¹)	R^2
0.12	46.99	0.898	0.003	55.5	0.999

3.2.2. Adsorption Isotherms

Isotherm adsorption modeling makes it possible to determine the various equilibrium parameters, understand the degree of affinity and interpret interaction mechanisms between the adsorbent and adsorbate. Numerous models have been developed in the literature, taking into account parameters such as the number of layers of adsorbed molecules, surface heterogeneity and binding energies [29]. Langmuir and Freundlich isotherm models are the most frequently used due to their simplicity and consistency. The adsorption mechanism of AO7 by AC was analyzed at three different temperatures using these two models. Figure 8 presents the data non-linearized and the corresponding fitted theoretical curves. The optimized parameter values obtained for Equations (5) and (6) are listed in Table 7.

The experimental results fit better with the Langmuir model based on homogeneous monolayer sorption ($R^2 = 0.9877$) than with the Freundlich model based on heterogeneous multilayer sorption at all temperatures. As a result, AO7 molecules are assumed to disperse into monolayers on adsorption sites that are identical in terms of energy and without electrostatic interactions between them [18]. The parameter R_L is a measure of the separation factor between the adsorbate and adsorbent in a system. A value between 0 and 1 indicates a favorable adsorption process, while $R_L > 1$ represents unfavorable adsorption. When R_L

= 1, adsorption is linear, and when its value is zero, the adsorption process is irreversible. The separation constant obtained by modeling in Table 7 ($R_L = 0.178 - 0.223 \ll 1$) suggests a very strong but still reversible adsorption of AO7 by the AC prepared in this work.

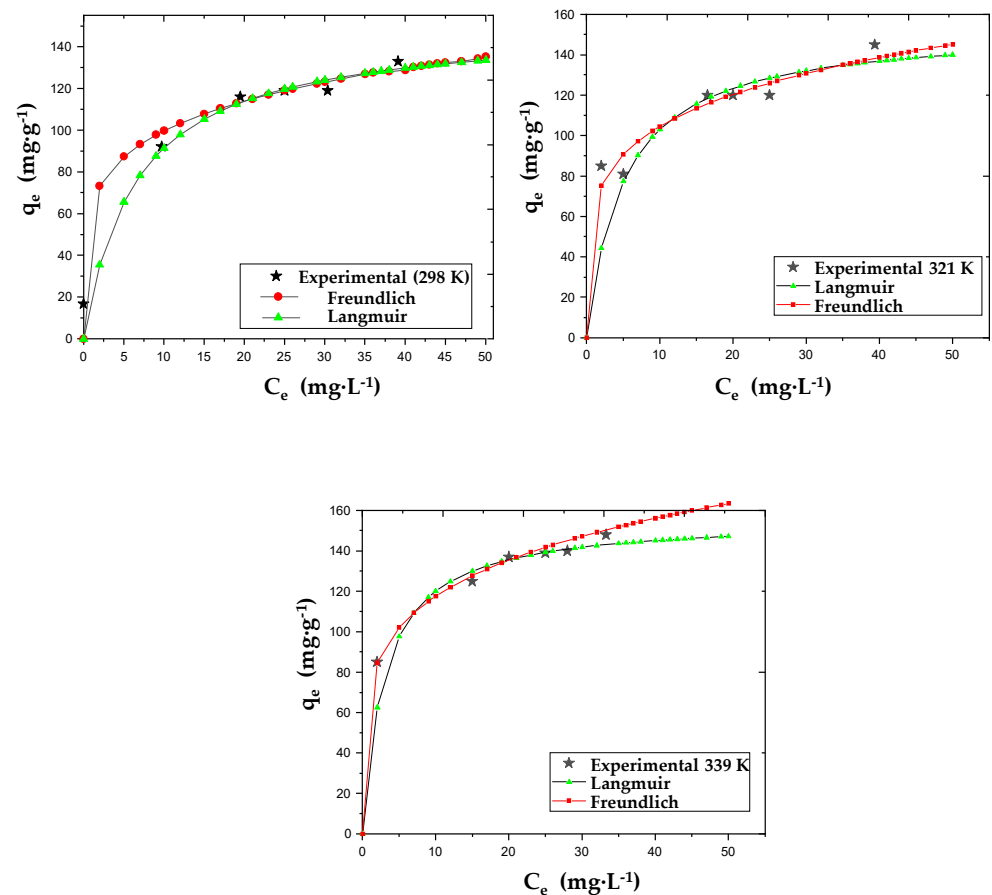


Figure 8. Non-linearized data of the AO7 adsorption isotherm on AC at three different temperatures and the corresponding fitted theoretical curves using the Langmuir and Freundlich models.

Table 7. Isotherm modeling parameters for AO7 adsorption.

T (K)	Langmuir			R_L	Freundlich		
	K_L ($L \cdot mol^{-1}$)	q_{max} ($mg \cdot g^{-1}$)	R^2		K_F ($L \cdot g^{-1})(L \cdot mg^{-1})^{1/n}$	$1/n$	R^2
298	0.154	151.51	0.9905	0.178	64.24	0.192	0.9852
321	0.203	153.85	0.9817	0.247	65.39	0.203	0.9369
339	0.349	156.25	0.9904	0.223	73.48	0.204	0.9579

3.2.3. Adsorption Thermodynamics

Thermodynamic factors, including standard free energy (ΔG°), enthalpy (ΔH°) and entropy (ΔS°), are the key parameters in understanding the adsorption reaction. It is then possible to gain deeper insight by identifying the spontaneity, heat exchange and degree of disorder of the process. Table 8 presents the values obtained in the temperature range 298–339 K using Equations (7)–(9).

The results led to the following conclusions:

The negative ΔG° values indicate that the adsorption process is favorable and spontaneous within the selected temperature range. The ΔG° values become more negative with the increasing temperature, suggesting that the adsorption process is facilitated. This effect

could be due to the widening of the AC pores with the increasing temperature, resulting in an easier diffusion of AO7 molecules and greater accessibility to adsorption sites located within the AC [52,54].

The positive ΔS° value indicates that the AO7 adsorption process is characterized by increased disorder in the interaction between dye molecules and the AC surface. A similar result has been reported for AO7 adsorption on AC from algae [18]. Adsorption is generally considered to decrease the number of degrees of freedom by reducing the adsorbate movement, resulting in a negative ΔS° value. The AO7 molecule is hydrophobic by nature (Table 1) and is assumed to be solubilized in water as small micellar aggregates. It can therefore be assumed that adsorption of an isolated molecule on the AC interface increases the degree of freedom, which may explain the positive value of ΔS° obtained.

The positive ΔH° value indicates that the dye adsorption process is endothermic in nature. Based on the ΔH° values, it can be deduced that the adsorption is predominantly physisorption through interactions between AO7 molecules and AC active sites such as hydrogen bonds and π - π interactions. This is confirmed by the fact that the ΔH° value is less than $40 \text{ kJ}\cdot\text{mol}^{-1}$ [55,56].

Table 8. Thermodynamic parameters for AO7 adsorption on AC.

Thermodynamic Parameters		ΔG° ($\text{kJ}\cdot\text{mol}^{-1}$)		ΔH° ($\text{kJ}\cdot\text{mol}^{-1}$)	ΔS° ($\text{J}\cdot(\text{mol}\cdot\text{K})^{-1}$)
T ($^\circ\text{K}$)	298	321	339		
	-7.43	-9.17	-10.53	15.12	75.65

3.3. Adsorption Mechanism

Previous studies have shown that dye adsorption on activated carbon is influenced by various factors, such as electrostatic attraction, hydrogen bonding, Van der Waals interactions and π - π interactions. Interestingly, adsorption of the anionic dye occurs at pH values higher than the pH_{PZC} of AC, while its surface charge is, on average, negative. Under these operating conditions, the predominant electrical interactions are repulsive, making adsorption unfavorable or limited even if a number of positive charges are present. This means that electrostatic interactions cannot be the main mechanism of AO7 adsorption and suggests the involvement of other types of interactions [18]. One possible mechanism is hydrogen bonding, as shown by the analysis of the FTIR spectra (Figure 1). The characteristic peak for hydroxyl groups showed a red shift (move from 3400 cm^{-1} to 3300 cm^{-1}) and broadening after AO7 adsorption, pointing to hydrogen bonding between the hydroxyl groups on the AC surface and AO7. In addition, π - π interactions between the adsorbents and dye molecules seem to play a crucial role in the AO7 adsorption process. This is also supported by the FTIR analysis, which revealed a weakening of the absorption intensity and a broadening of the characteristic C=C peak (1600 cm^{-1}) in the AC spectrum after AO7 adsorption (Figure 1), suggesting an interaction between the π -electron system of the AC structure and the aromatic rings of the AO7 dye molecules (Table 1) [55,56]. This is in perfect agreement with the endothermic nature of adsorption and the ΔH° value marking a physisorption mechanism and π - π -type interactions, as mentioned above. Figure 9 presents the proposed interaction mechanisms occurring during the AO7 adsorption on AC prepared from SCGs in this work.

3.4. Experimental Design and Response Surface Plots of AO7 Removal

Preliminary experiments showed that contact time, dye concentration and adsorbent dose were the key factors to be optimized. Although pH and temperature also had an influence, they were not of primary importance for the adsorption of AO7 on the AC prepared in this work. Therefore, to save time, these two parameters were kept at 7.5 and about $25 \text{ }^\circ\text{C}$, while only the first three parameters mentioned were varied.

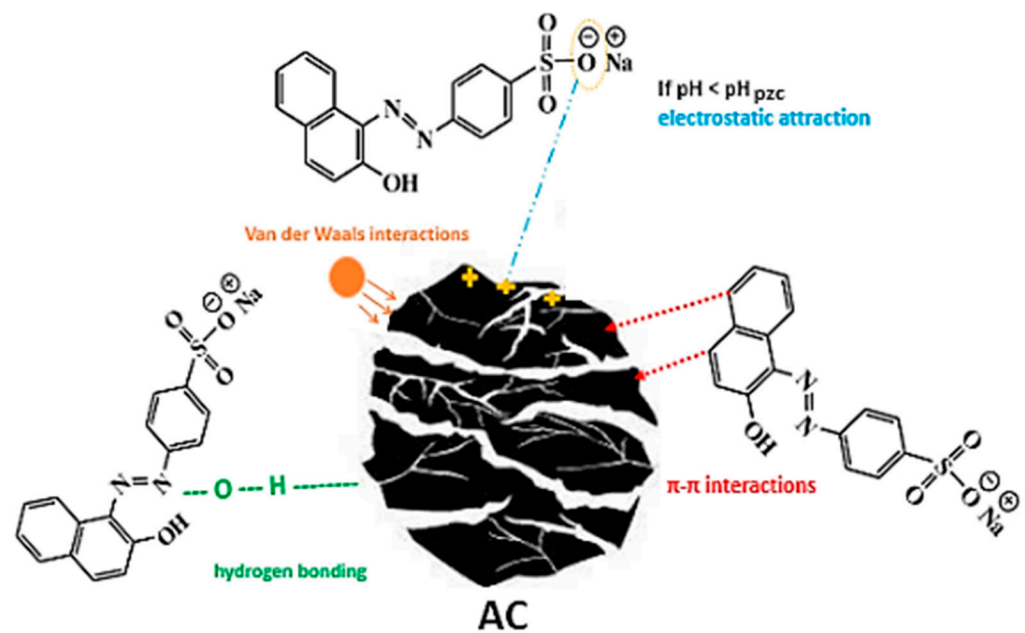


Figure 9. Proposed adsorption mechanisms of AO7 dye onto the activated carbon (AC).

3.4.1. Statistical Analysis of the Derived Response Surface Model

In order to determine the optimum experimental conditions for AO7 removal efficiency by AC (output variable response) and to elucidate the weight of the different input parameters (X_1 : contact time, X_2 : dye concentration, and X_3 : adsorbent dose), batch adsorption experiments were carried out using the Box–Behnken design method as part of the RSM model. A series of 15 experiments was conducted according to a customized design, and the experimental- and model-predicted responses are summarized in Table 9. The last column shows the residual calculated as the difference between the experimental responses and those predicted by the model. Depending on the value of the input factors, the percentage of dye removal varies between 15 and 98%, with residual values well below 4%.

Table 9. Box–Behnken design and comparison of experimental- and model-predicted results for AO7 adsorption using AC.

Test Number	X_1 (min)	Factors		Response Y		Residual (% Removal)
		X_2 (mg·L ⁻¹)	X_3 (g·L ⁻¹)	Experimental (% Removal)	Predicted (% Removal)	
1	60 (+1)	50 (+0)	0.100 (−1)	49.3	47.15	2.15
2	35 (+0)	50 (+0)	0.250 (+0)	84.0	85.45	−1.45
3	60 (+1)	10 (−1)	0.250 (+0)	97.2	97.19	0.0063
4	10 (−1)	90 (+1)	0.250 (+0)	47.0	45.55	1.45
5	35 (+0)	50 (+0)	0.250 (+0)	84.0	85.44	−1.44
6	10 (−1)	50 (+0)	0.100 (−1)	36.3	34.09	2.21
7	60 (+1)	90 (+1)	0.250 (+0)	51.0	49.56	1.44
8	35 (+0)	90 (+1)	0.400 (+1)	54.7	56.87	−2.17
9	10 (−1)	10 (−1)	0.250 (+0)	77.7	78.02	−0.3233
10	60 (+1)	50 (+0)	0.400 (+1)	98.0	94.39	3.61
11	35 (+0)	10 (−1)	0.100 (−1)	67.0	67.01	−0.0063
12	35 (+0)	10 (−1)	0.400 (+1)	98.0	100.16	−2.16
13	35 (+0)	50 (+0)	0.250 (+0)	81.1	78.02	3.1
14	35 (+0)	90 (+1)	0.100 (−1)	15.0	18.61	−3.61
15	10 (−1)	50 (+0)	0.400 (+1)	75.3	78.02	−2.72

Table 10 presents the analysis of variance (ANOVA) of the regression parameters of the quadratic response surface models predicted for the percent of dye removal. The F -value of

66.94 and the adjusted regression coefficient above 99% indicate that the model equation is highly significant. Furthermore, there is only a small probability of 0.01% that this F -value is due to noise [52].

Table 10. Analysis of variance for the adsorption of AO7 dye by AC.

Source	Sum of Squares	Degree of Freedom	Mean of Squares	F -Value	p -Value		R^2	R^2_{adj}
Model	8485.68	9	942.85	66.94	0.0001	significant	0.9918	0.9770
Error	17.39	2	8.69					

This analysis also makes it possible to determine the weight of the input parameters and their interactions through the polynomial coefficients of the model (Table 11). It appears from the F -values that X_1 , X_2 , X_3 , X_1X_3 , X_2X_3 , X_1^2 and X_3^2 are the most significant terms in the model. In addition, p -values greater than 0.100 indicate that X_1X_2 and X_2^2 do not significantly contribute to the removal efficiency of AO7. Consequently, the polynomial Equation (10) can simply be written as follows:

$$Y(\%) = 78.02 + 6.54 X_1 - 26.49 X_2 + 11.4 X_3 + 7.75 X_1 X_3 + 12.8 X_2 X_3 - 10.63 X_1^2 - 7.64 X_3^2 \quad (11)$$

Table 11. Estimated polynomial coefficients for the adsorption of AO7 dye by AC.

Coefficient	Estimated Coefficient	F -Value	p -Value
a_0	78.02		
a_1	6.54	24.32	0.0044
a_2	-26.49	398.7	<0.0001
a_3	11.40	73.82	0.0004
$a_1 a_2$	-0.813	0.188	0.6831
$a_1 a_3$	7.75	17.04	0.0091
$a_2 a_3$	12.80	46.53	0.001
a_1^2	-10.63	29.61	0.0028
a_2^2	-1.08	0.307	0.6031
a_3^2	-7.64	15.3	0.0113

For the purpose of process optimization, Equation (11) of the model shows the extent to which dye removal efficiency is affected by the various input factors considered through their linear and quadratic terms, as well as their mutual interactions. Negative coefficients indicate that the corresponding factors have a negative impact on the removal efficiency [32]. The factor (X_2) is the most influential parameter: the higher the dye concentration, the lower the removal efficiency (Y). Contact time (X_1) and adsorbent dose (X_3) have antagonistic effects.

As mentioned above, the regression coefficient R^2 obtained in this study was 0.9918, indicating that the developed customized model accounted for about 99% of the variability observed in the experimental data. In addition, the adjusted regression coefficient R^2_{adj} was 0.9770, which implies that nearly 98% of the variability, given the number of variables and degrees of freedom, can be explained by the model. Figure 10 compares actual values with predicted model-derived responses for AO7 removal, illustrating the fit between the optimization model and experimental data. The proximity of the data points to the diagonal line in the plot of actual versus predicted values and indicates the suitability of the model developed. This means that the statistical model effectively captures the correlation among the three factors investigated in AO7 removal. It was concluded that the Equation (11) model is highly predictive and appropriate to accurately represent the relationship between the variables considered [40].

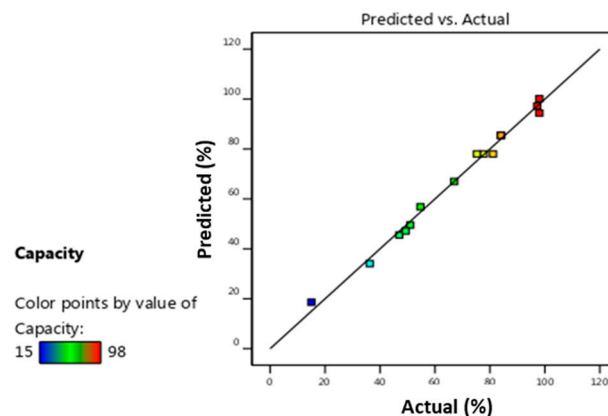


Figure 10. The removal efficiency predicted from Equation (11) (Y) versus the actual data (R) from Equation (2) for AO7 adsorption using AC.

3.4.2. Interaction Effect of Variables on Dye Removal Efficiency of AO7 Dye by AC

The 3D response surface plots and contour graphs for the removal efficiency of AO7 when using AC give a graphical interpretation of the second-order model equation to examine the relationship between the different factors considered in the adsorption process.

- Dye concentration and adsorbent dosage.** Figure 11 illustrates the interaction effects of the dye concentration and adsorbent dose on the removal efficiency at a fixed time of 35 min. This shows that better responses were observed with higher adsorbent masses. This result shows the importance of the factors involving the input parameter X_3 in Equation (11). Increasing the amount of AC enhances the availability of active adsorption sites for dye binding, thus promoting the removal process [42]. On the other hand, increasing the dye concentration from 10 to 90 mg·L⁻¹ while maintaining the AC dose at 0.250 g·L⁻¹ results in a reduction in removal from 98% to 60%. The high removal efficiency of adsorbates at low concentrations can be attributed to the large number of adsorption sites available. This allows greater accessibility and facilitated adsorption, leading to the removal of a greater proportion of adsorbate from solution. It is important to note that the number of available sites is a major factor in determining the adsorption efficiency Y , showing the antagonistic impact of input parameters X_2 and X_3 in Equation (11). As the initial concentration of AO7 (X_2) increases, the number of available adsorption sites decreases, reducing the efficiency of adsorption removal [57].
- Adsorbent dose and contact time.** The 3D response surface and contour map, illustrating the interaction effects of the contact time (X_1) and adsorbent dose (X_3) on dye removal efficiency (Y) at a fixed dye concentration (50 mg·L⁻¹), are shown in Figure 12. It can be seen that, for an AC adsorbent dose of less than 0.250 g·L⁻¹, the contact time has a negligible effect on AO7 retention, as the available active sites are few in number and rapidly saturated. On the other hand, at a dose higher than 0.250 g·L⁻¹, AO7 retention increases with the contact time up to 40 min, when retention becomes stable as all active sites are saturated and equilibrium is reached [58].
- Contact time and dye concentration.** The 3D graph and contour map shown in Figure 13 illustrate the combined influence of dye concentration (X_2) and contact time (X_1) on the removal efficiency (Y). The experiment was carried out with a constant AC dosage of 0.250 mg·L⁻¹. The contour map reveals an almost constant removal efficiency, indicating that AO7 adsorption remained relatively unchanged with the varying contact times over the range studied. This lack of significant change in removal with the contact time suggests rapid adsorption kinetics. However, increasing the dye concentration and maintaining a constant contact time leads to local saturation of the most easily accessible active sites. This phenomenon causes the driving force to remain at the same level until the adsorption process reaches equilibrium [59]. In

general, the interaction of the dye concentration and time of contact has a negative effect on the response variable.

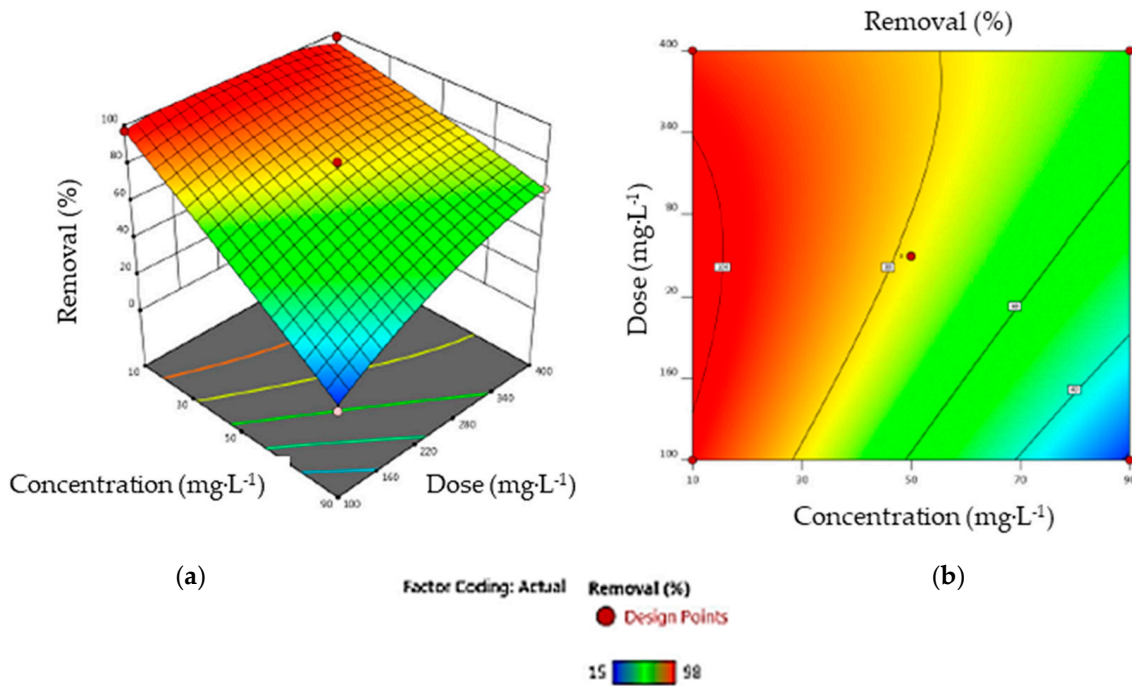


Figure 11. (a) The response surface and (b) the contour map showing the interaction of AO7 concentration and AC dosage (input parameters X_2 and X_3 in Equation (11), respectively) on dye removal.

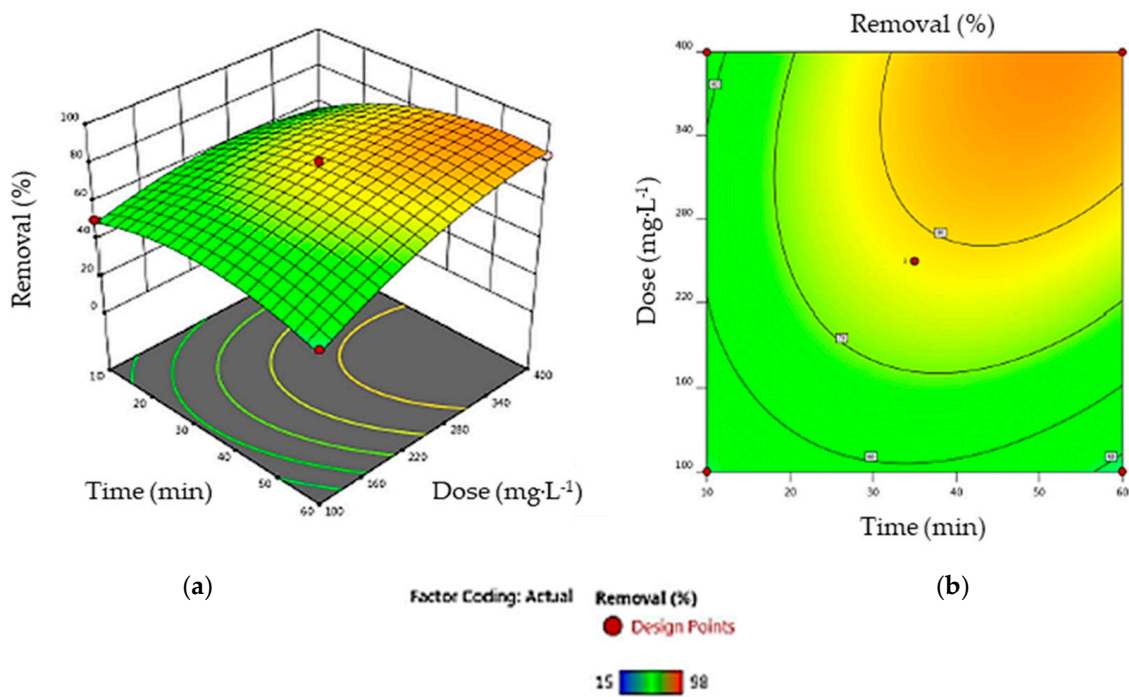


Figure 12. (a) The response surface and (b) the contour map showing the interaction of contact time and AC dosage (input parameters X_1 and X_3 in Equation (11), respectively) on dye removal.

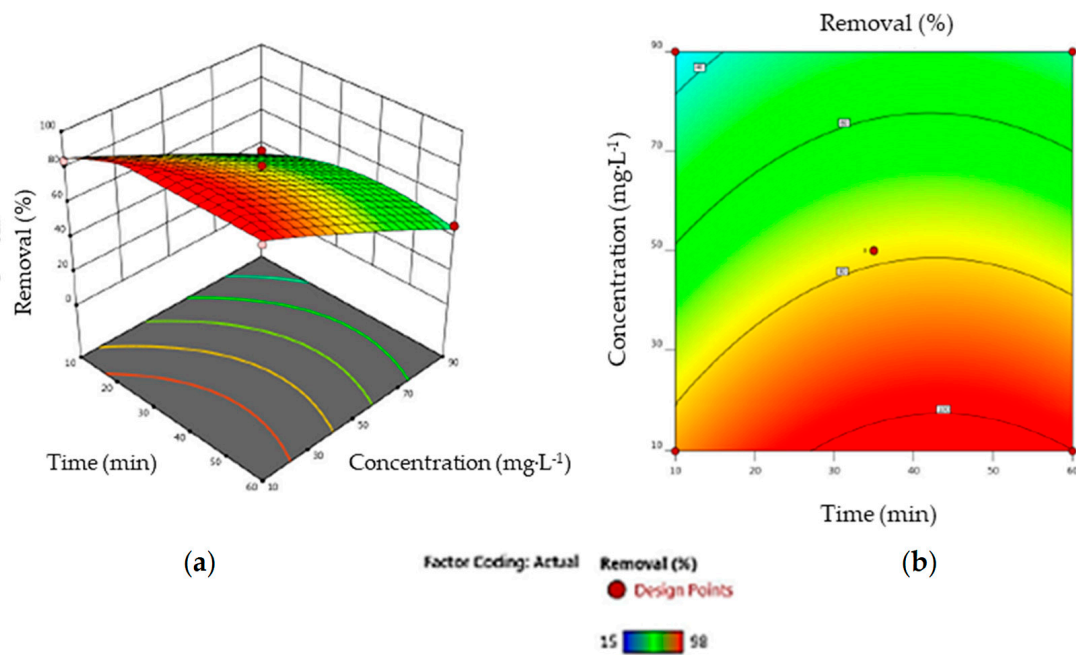


Figure 13. (a) The response surface and (b) the contour map showing the interaction of the AO7 concentration and contact time (input parameters X_2 and X_1 in Equation (11), respectively).

3.4.3. Process Optimization

The optimum conditions in the range studied predicted by the model to ensure maximum AO7 removal were an adsorbent dose of $0.285 \text{ g}\cdot\text{L}^{-1}$, a dye concentration of $20 \text{ mg}\cdot\text{L}^{-1}$ and a contact time of 40 min. These conditions were expected to lead to a dye removal efficiency of 98%. An experiment was carried out using these specified parameters. The obtained results showed a discoloration rate of 97.6%, corresponding closely to the value predicted by the model. The agreement between experimental and predicted values confirms the accuracy and reliability of the customized model. Consequently, the model is considered a reliable tool for predicting and monitoring AO7 removal efficiency using AC.

To test the reusability of AC after dye removal, desorption experiments were carried out with 50 wt.% ethanol at room temperature for 2 h. The adsorbent obtained was then recycled four times to remove AO7 (Figure 14).

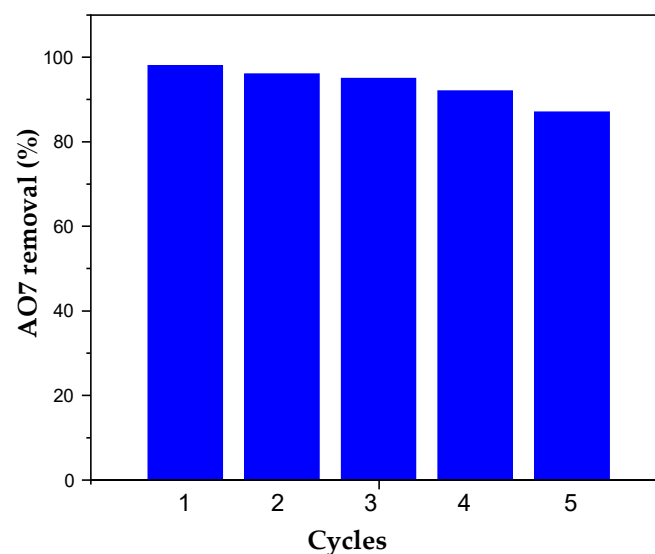


Figure 14. Removal rate of AO7 and recovery efficiency of AC after 5 adsorption/regeneration cycles.

As can be seen, the results show that AC after regeneration can be reused with a capacity loss of only a few percent for the first three cycles. A more significant drop was observed for the subsequent cycles. This could be due to irreversible adsorption on high-affinity sites. Dye accumulation on the adsorbent surface would partially limit the availability of other adsorption sites. However, given the low cost of this adsorbent, reuse over a small number of cycles should be sufficient for large-scale use.

3.5. Comparative Study

Table 12 compares the efficiency of the different adsorbents used to remove AO7 dye from aqueous solution reported in the literature [18,43,58,60–63]. As shown in this survey, the AC obtained from the SCGs had an excellent affinity for AO7 dye removal (in terms of adsorption capacity and kinetics) and compared favorably with the other low-cost activated carbon and bio-adsorbents. The dose of adsorbent required is comparatively low ($0.285 \text{ g}\cdot\text{L}^{-1}$), and the contact time is equally short (40 min), which may be explained by the high accessibility of adsorption sites despite the low specific surface area (BET) of AC compared to activated carbon produced at higher temperatures. These operating conditions are very attractive and advantageous for a dye removal process using adsorption on activated carbon. Consequently, AC prepared from SCGs according to the procedure described in this work is a promising adsorbent with great potential for the decolorization of wastewater from the textile industry.

Table 12. Comparative study of the adsorption of AO7 dye on various bio-sorbents from the literature.

Bio-Sorbent	Experimental Conditions				Results		Lit.
	pH	AO7 ($\text{mg}\cdot\text{L}^{-1}$)	Adsorbent Dose ($\text{g}\cdot\text{L}^{-1}$)	Contact Time (min)	Removal (%)	Capacity ($\text{mg}\cdot\text{g}^{-1}$)	
Bifurcaria bifurcate activated carbon	7.5	10	0.2	120	88.8	82.56	[18]
Activated carbon based on grape marc	2	150	2	180	-	140.5	[43]
Aloe vera leaves	2	50	2.5	360	-	15.9	[58]
Coconut coir activated carbon	3	40	6	120	99.5	13.16	[60]
Activated carbon from Pisum sativum pods	1.5	100	2	95.7	~100	473.93	[61]
Spent brewery grains	4.5	60	3.75	60	>90	30.5	[62]
Activated carbon from Casuarina wood	2.8	25	2	90	83.4	9.51	[63]
AC from SCG	7.5	20	0.285	40	98	119.51	¹

¹ This study.

4. Conclusions

A simple and reproducible procedure for preparing activated carbon (AC) from used coffee grounds was successfully developed involving chemical activation with a small amount of H_3PO_4 at the relatively low temperature of 600°C , making it an inexpensive material. It was found that the two batches of AC prepared exhibited excellent and similar adsorption properties for AO7 removal from aqueous solutions. A comprehensive adsorption study was conducted, including kinetics, thermodynamics, mechanism and process optimization.

Analysis of surface chemical functions by FTIR and a thermodynamic study revealed that AO7 adsorbs to AC by spontaneous physisorption involving mainly hydrogen bonds and π - π interactions. The modeling of AO7 adsorption by AC showed that experimental kinetic and isotherm data fitted best with the pseudo-second-order model and the Langmuir model, respectively. To optimize AO7 removal by AC, experimental design methodology was applied, allowing the influence of specific parameters such as contact time, dye concentration and adsorbent quantity to be determined. The optimal design model fitted with the experimental data showed a high coefficient of determination ($R^2 = 0.9918$) and an adjusted R^2 coefficient of 0.9770, indicating that it is a robust predictive model. In addition, the statistical significance was validated by a p -value associated with the model of less than 0.05. The optimal conditions for the nearly complete removal of AO7 (98%) at a concentration of $20 \text{ mg}\cdot\text{L}^{-1}$, predicted by the model and experimentally tested, required a contact time of 40 min and an adsorbent dosage of $0.285 \text{ g}\cdot\text{L}^{-1}$.

The adsorption of dyes contained in textile industry wastewater using inexpensive, locally available activated carbon prepared from spent coffee grounds therefore appears to be a promising and effective treatment for pollution challenges, with a strong potential for scale-up. A comprehensive study of the adsorption properties with real effluents is currently underway and will be published in the near future.

Author Contributions: Conceptualization, A.D. and R.B.A.; methodology, A.A. and L.D.; validation, A.D. and R.B.A.; investigation, F.A.; data curation, F.A., A.A. and L.D.; writing—original draft preparation, F.A., A.A. and R.B.A.; writing—review and editing, A.D.; supervision, A.D. and R.B.A. All authors have read and agreed to the published version of the manuscript.

Funding: This research received no external funding.

Institutional Review Board Statement: Not applicable.

Informed Consent Statement: Not applicable.

Data Availability Statement: Dataset available on request from the corresponding authors.

Acknowledgments: The authors gratefully acknowledge the characterization platform of Institut Européen des Membranes for the analyses and F.A. the Research Unit “Advanced Technologies for Environment and Smart Cities” for her grant.

Conflicts of Interest: The authors declare no conflicts of interest.

References

1. Ahmed, J.; Thakur, A.; Goyal, A. Industrial Wastewater and Its Toxic Effects. In *Biological Treatment of Industrial Wastewater*; Shah, M.P., Ed.; The Royal Society of Chemistry: London, UK, 2021; pp. 1–14. [\[CrossRef\]](#)
2. Ullah Khan, W.; Ahmed, S.; Dhoble, Y.; Madhav, S. A critical review of hazardous waste generation from textile industries and associated ecological impacts. *J. Indian Chem. Soc.* **2023**, *100*, 100829. [\[CrossRef\]](#)
3. Panhwar, A.; Jatoi, S.A.; Mazari, S.A.; Kandhro, A.; Rashid, U.; Qaisar, S. Water resources contamination and health hazards by textile industry effluent and glance at treatment techniques: A review. *Waste Manag. Bull.* **2024**, *1*, 158–163. [\[CrossRef\]](#)
4. Subramaniam, R.; Ponnusamy, S.K. Novel adsorbent from agricultural waste (cashew NUT shell) for Methylene Blue dye removal: Optimization by response surface methodology. *Water Resour. Ind.* **2015**, *11*, 64–70. [\[CrossRef\]](#)
5. Katheresan, V.; Kansedo, J.; Lau, S.Y. Efficiency of various recent wastewater dye removal methods: A review. *J. Environ. Chem. Eng.* **2018**, *6*, 4676–4697. [\[CrossRef\]](#)
6. Hani, K.A.; Hani, Z.; Ben Amar, R. Evaluation of the use of agricultural waste materials as low-cost and eco-friendly sorbents to remove dyes from water: A review. *Desalin. Water Treat.* **2023**, *302*, 231–252. [\[CrossRef\]](#)
7. Zenebe, A.; Yimer, A.M.; Kuzhunellil, S.; Demissie, H. Green synthesis of magnetic nanocomposite by Cordia Africana (CA) leave extract for the treatment of Methylene Blue contaminated water. *Adv. Chem. Eng.* **2021**, *8*, 100193. [\[CrossRef\]](#)
8. Yagub, M.T.; Sen, T.K.; Afroze, S.; Ang, H.M. Dye and its removal from aqueous solution by adsorption: A review. *Adv. Colloid Interface Sci.* **2014**, *209*, 172–184. [\[CrossRef\]](#) [\[PubMed\]](#)
9. Foo, K.Y.; Hameed, B.H. An overview of dye removal via activated carbon adsorption process. *Desalin. Water Treat.* **2010**, *19*, 255–274. [\[CrossRef\]](#)
10. Demirbas, A. Agricultural based activated carbons for the removal of dyes from aqueous solutions: A review. *J. Hazard. Mater.* **2009**, *167*, 1–9. [\[CrossRef\]](#)
11. Shakoor, S.; Nasar, A. Adsorptive treatment of hazardous Methylene Blue dye from artificially contaminated water using Cucumis sativus peel waste as a low-cost adsorbent. *Groundw. Sustain. Dev.* **2017**, *5*, 152–159. [\[CrossRef\]](#)
12. Oyarce, E.; Pizarro, G.D.C.; Oyarzún, D.P.; Martín-Trasanco, R.; Sánchez, J. Adsorption of Methylene Blue in aqueous solution using hydrogels based on 2-hydroxyethyl methacrylate copolymerized with itaconic acid or acrylic acid. *Mater. Today Commun.* **2020**, *25*, 101324. [\[CrossRef\]](#)
13. Liu, X.; Tian, J.; Li, Y.; Sun, N.; Mi, S.; Xie, Y.; Chen, Z. Enhanced dyes adsorption from wastewater via Fe₃O₄ nanoparticles functionalized activated carbon. *J. Hazard. Mater.* **2019**, *373*, 397–407. [\[CrossRef\]](#) [\[PubMed\]](#)
14. Berradi, M.; Hsissou, R.; Khudhair, M.; Assouag, M.; Cherkaoui, O.; El Bachiri, A.; El Harfi, A. Textile finishing dyes and their impact on aquatic environs. *Heliyon* **2019**, *5*, e02711. [\[CrossRef\]](#) [\[PubMed\]](#)
15. Perez-Calderon, J.; Marin-Silva, D.A.; Zaritzky, N.; Pinotti, A. Eco-friendly PVA-chitosan adsorbent films for the removal of azo dye Acid Orange 7: Physical cross-linking, adsorption process, and reuse of the material. *Adv. Ind. Eng. Polym. Res.* **2023**, *6*, 239–254. [\[CrossRef\]](#)
16. Nistor, M.-A.; Halip, L.; Muntean, S.G.; Kurunczi, L.; Costișor, O. Modeling and optimization of Acid Orange 7 adsorption process using magnetite/carbon nanocomposite. *Sustain. Chem. Pharm.* **2022**, *29*, 100778. [\[CrossRef\]](#)
17. Zhang, L.; Cheng, Z.; Guo, X.; Jiang, X.; Liu, R. Process optimization, kinetics and equilibrium of orange G and acid orange 7 adsorptions onto chitosan/surfactant. *J. Mol. Liq.* **2014**, *197*, 353–367. [\[CrossRef\]](#)

18. Bouzikri, S.; Ouasfi, N.; Khamliche, L. *Bifurcaria bifurcata* activated carbon for the adsorption enhancement of Acid Orange 7 and Basic Red 5 dyes: Kinetics, equilibrium and thermodynamics investigations. *Energy Nexus* **2022**, *7*, 100138. [[CrossRef](#)]
19. Bouhaik, I.S.; Meliani, M.H.; Suleiman, R.K.; Saleh, T.A. Mechanistic insights into acid orange 7 azo dye (AO7) reduction using DFT calculations. *Polyhedron* **2023**, *245*, 116648. [[CrossRef](#)]
20. Ye, Q.; Wu, H.; Li, J.; Huang, Y.; Zhang, M.; Yi, Q.; Yan, B. Preparation of 1,8-dichloroanthraquinone/graphene oxide/poly(vinylidene fluoride) (1,8-AQ/GO/PVDF) mediator membrane and its application to catalyzing biodegradation of azo dyes. *Ecotoxicol. Environ. Saf.* **2023**, *268*, 115681. [[CrossRef](#)]
21. Shindhal, T.; Rakholiya, P.; Varjani, S.; Pandey, A.; Ngo, H.H.; Guo, W.; Ng, H.Y.; Taherzadeh, M.J. A critical review on advances in the practices and perspectives for the treatment of dye industry wastewater. *Bioengineered* **2021**, *12*, 70–87. [[CrossRef](#)]
22. Bai, X.; Sun, H.; Sun, J.; Zhu, Z. Efficient removal of sixteen priority polycyclic aromatic hydrocarbons from textile dyeing sludge using electrochemical Fe²⁺-activated peroxymonosulfate oxidation—A green pretreatment strategy for textile dyeing sludge toxicity reduction. *J. Hazard. Mater.* **2022**, *435*, 129087. [[CrossRef](#)] [[PubMed](#)]
23. Ihaddaden, S.; Aberkane, D.; Boukerroui, A.; Robert, D. Removal of methylene blue (basic dye) by coagulation-flocculation with biomaterials (bentonite and *Opuntia ficus indica*). *J. Water Process Eng.* **2022**, *49*, 102952. [[CrossRef](#)]
24. Khmiri, Y.; Attia, A.; Aloulou, H.; Dammak, L.; Baklouti, L.; Ben Amar, R. Preparation and Characterization of New and Low-Cost Ceramic Flat Membranes Based on Zeolite-Clay for the Removal of Indigo Blue Dye Molecules. *Membranes* **2023**, *13*, 865. [[CrossRef](#)]
25. Benkhaya, S.; M'rabet, S.; Hsissou, R.; El Harfi, A. Synthesis of new low-cost organic ultrafiltration membrane made from Polysulfone/Polyetherimide blends and its application for soluble azoic dyes removal. *J. Mater. Res. Technol.* **2020**, *9*, 4763–4772. [[CrossRef](#)]
26. Sun, C.; Liu, H. Room temperature route to silsesquioxane-based porphyrin functional NIR porous polymer for efficient photodegradation of azo-dyes under sunlight. *Next Mater.* **2024**, *2*, 100123. [[CrossRef](#)]
27. Pereira, A.G.B.; Rodrigues, F.H.A.; Paulino, A.T.; Martins, A.F.; Fajardo, A.R. Recent advances on composite hydrogels designed for the remediation of dye-contaminated water and wastewater: A review. *J. Clean. Prod.* **2021**, *284*, 124703. [[CrossRef](#)]
28. Samadi, A.; Wang, Z.; Wang, S.B.; Nataraj, S.K.; Kong, L.; Zhao, S. Polyaniline-based adsorbents for water treatment: Roles of low-cost materials and 2D materials. *Chem. Eng. J.* **2023**, *478*, 147506. [[CrossRef](#)]
29. Husien, S.; El-taweel, R.M.; Salim, A.I.; Fahim, I.S.; Said, L.A.; Radwan, A.G. Review of activated carbon adsorbent material for textile dyes removal: Preparation, and modelling. *Curr. Res. Green Sustain. Chem.* **2022**, *5*, 100325. [[CrossRef](#)]
30. Gayathiri, M.; Pulingam, T.; Lee, K.T.; Sudesh, K. Activated carbon from biomass waste precursors: Factors affecting production and adsorption mechanism. *Chemosphere* **2022**, *294*, 133764. [[CrossRef](#)]
31. Jung, K.-W.; Choi, B.H.; Hwang, M.-J.; Jeong, T.-U.; Ahn, K.-H. Fabrication of granular activated carbons derived from spent coffee grounds by entrapment in calcium alginate beads for adsorption of acid orange 7 and methylene blue. *Bioresour. Technol.* **2016**, *219*, 185–195. [[CrossRef](#)]
32. Azzouni, D.; Baragh, F.; Mahmoud, A.M.; Alanazi, M.M.; Rais, Z.; Taleb, M. Optimization of methylene blue removal from aqueous solutions using activated carbon derived from coffee ground pyrolysis: A response surface methodology (RSM) approach for natural and cost-effective adsorption. *J. Saudi Chem. Soc.* **2023**, *27*, 101695. [[CrossRef](#)]
33. Klosek-Wawrzyn, E.; Frac, M.; Pichór, W. Influence of pregranulation and low-pressure compaction on the properties of ceramic materials incorporating clay and spent coffee grounds. *Appl. Clay Sci.* **2023**, *245*, 107154. [[CrossRef](#)]
34. McNutt, J.; He, Q. Spent Coffee Grounds: A Review on Current Utilization. *J. Ind. Eng. Chem.* **2019**, *71*, 78–88. [[CrossRef](#)]
35. Ma, W.; Fan, J.; Cui, X.; Wang, Y.; Yan, Y.; Meng, Z.; Gao, H.; Lu, R.; Zhou, W. Pyrolyzing Spent Coffee Ground to Biochar Treated with H₃PO₄ for the Efficient Removal of 2,4-Dichlorophenoxyacetic Acid Herbicide: Adsorptive Behaviors and Mechanism. *J. Environ. Chem. Eng.* **2023**, *11*, 109165. [[CrossRef](#)]
36. Obar, F.; Pradhan, S.; Mackey, H.R.; McKay, G. Removal of Lithium from Aqueous Solution by Spent Coffee Ground Activated Biochar. *Process Saf. Environ. Prot.* **2024**, *184*, 680–689. [[CrossRef](#)]
37. Bose, S.; Kirk, R.D.; Maslen, H.; Pardo Islas, M.A.; Smith, B.; Dugmore, T.I.J.; Matharu, A.S. Mesoporous-Rich Calcium and Potassium-Activated Carbons Prepared from Degreased Spent Coffee Grounds for Efficient Removal of MnO₄²⁻ in Aqueous media. *RSC Adv.* **2022**, *12*, 19417–19423. [[CrossRef](#)] [[PubMed](#)]
38. Sani, M.N.H.; Amin, M.; Siddique, A.B.; Nasif, S.O.; Ghaley, B.B.; Ge, L.; Wang, F.; Yong, J.W.H. Waste-Derived Nanobiochar: A New Avenue towards Sustainable Agriculture, Environment, and Circular Bioeconomy. *Sci. Total Environ.* **2023**, *905*, 166881. [[CrossRef](#)] [[PubMed](#)]
39. Solihat, N.N.; Hidayat, A.F.; Ilyas, R.A.; Thiagamani, S.M.K.; Azelee, N.I.W.; Sari, F.P.; Ismayati, M.; Bakshi, M.I.; Garba, Z.N.; Hussin, M.H.; et al. Recent Antibacterial Agents from Biomass Derivatives: Characteristics and Applications. *J. Bioresour. Bioprod.* **2024**, *in press*. [[CrossRef](#)]
40. Babakhani, A.; Sartaj, M. Optimization of Nickel(II) Adsorption by Sodium Tripolyphosphate Crosslinked Chitosan Using Response Surface Methodology (RSM). *Sustain. Chem. Environ.* **2023**, *2*, 100019. [[CrossRef](#)]
41. Ahmad, A.; Yadav, A.K. Parametric Analysis of Wastewater Electrolysis for Green Hydrogen Production: A Combined RSM, Genetic Algorithm, and Particle Swarm Optimization Approach. *Int. J. Hydrogen Energy* **2024**, *59*, 51–62. [[CrossRef](#)]
42. Nure, J.F.; Mengistu, A.; Abewaa, M.; Angassa, K.; Moyo, W.; Phiri, Z.; Mafa, P.J.; Kuvarega, A.T.; Nkambule, T.T.I. Adsorption of Black MNN Reactive Dye from Tannery Wastewater Using Activated Carbon of *Rumex Abyssinicus*. *J. Taiwan Inst. Chem. Eng.* **2023**, *151*, 105138. [[CrossRef](#)]

43. Al, K.; Kabakcı, S.B. Oxygen-Rich Precursors via Glycerol Organosolv Treatment: Preparation of Activated Carbon from Hazelnut Shell and Its Structural Components for Possible Use in Electrodes for Supercapacitors. *Int. J. Thermofluids* **2024**, *21*, 100588. [[CrossRef](#)]
44. Chavhan, M.P.; Slovák, V.; Siddiqi, H.; Mucha, M. Pyrolysis of Household Coffee Vis-à-Vis Tea Waste: A Detailed Insight into Physicochemical Properties, Kinetics, and Thermodynamics Study. *Chem. Eng. J. Adv.* **2024**, *17*, 100587. [[CrossRef](#)]
45. Bourahla, S.; Nemchi, F.; Belayachi, H.; Belayachi, A.; Harrats, C.; Belhakem, M. Removal of the AO7 Dye by Adsorption on Activated Carbon Based on Grape Marc: Equilibrium, Regeneration, and FTIR Spectroscopy. *J. Iran. Chem. Soc.* **2023**, *20*, 669–681. [[CrossRef](#)]
46. Dhelipan, M.; Arunchander, A.; Sahu, A.K.; Kalpana, D. Activated carbon from orange peels as supercapacitor electrode and catalyst support for oxygen reduction reaction in proton exchange membrane fuel cell. *J. Saudi Chem. Soc.* **2017**, *21*, 487–494. [[CrossRef](#)]
47. Keppetipola, N.; Maithri, M.; Dissanayake, P.; Karunarathne, B.; Dourges, M.A.; Talaga, D.; Servant, L.; Olivier, C.; Toupance, T.; Uchida, S.; et al. Graphite-type activated carbon from coconut shell: A natural source for eco-friendly non-volatile storage devices. *RSC Adv.* **2021**, *11*, 2854–2865. [[CrossRef](#)] [[PubMed](#)]
48. Lazzarini, A.; Piovano, A.; Pellegrini, R.; Agostini, G.; Rudiü, S.; Lambertia, C.; Groppo, E. Graphitization of activated carbons: A molecular-level investigation by INS, DRIFT, XRD and Raman techniques. *Phys. Procedia* **2016**, *85*, 20–26. [[CrossRef](#)]
49. Jedynek, K.; Szczepanik, B.; Rędzia, N.; Słomkiewicz, P.; Kolbus, A.; Rogala, P. Ordered mesoporous carbons for adsorption of paracetamol and non-steroidal anti-inflammatory drugs: Ibuprofen and naproxen from aqueous solutions. *Water* **2019**, *11*, 1099. [[CrossRef](#)]
50. Schütz, T.; Dolinská, S.; Hudec, P.; Mockovčiaková, A.; Znamenáčková, I. Cadmium adsorption on manganese modified bentonite and bentonite–quartz sand blend. *Int. J. Miner. Process.* **2016**, *150*, 32–38. [[CrossRef](#)]
51. Dziejarski, B.; Hernández-Barreto, D.F.; Moreno-Piraján, J.C.; Giraldo, L.; Serafin, J.; Knutsson, P.; Andersson, K.; Krzyżyńska, R. Upgrading Recovered Carbon Black (rCB) from Industrial-Scale End-of-Life Tires (ELTs) Pyrolysis to Activated Carbons: Material Characterization and CO₂ Capture Abilities. *Environ. Res.* **2024**, *247*, 118169. [[CrossRef](#)]
52. Romdhani, M.; Attia, A.; Charcosset, C.; Mahouche-Chergui, S.; Ates, A.; Duplay, J.; Ben Amar, R. Optimization of Paracetamol and Chloramphenicol Removal by Novel Activated Carbon Derived from Sawdust Using Response Surface Methodology. *Sustainability* **2023**, *15*, 2516. [[CrossRef](#)]
53. Bernal, V.; Giraldo, L.; Moreno-Piraján, J.C. Physicochemical Properties of Activated Carbon: Their Effect on the Adsorption of Pharmaceutical Compounds and Adsorbate–Adsorbent Interactions. *C* **2018**, *4*, 62. [[CrossRef](#)]
54. Amellal, T.; Boukhalfa, N.; Meniai, A.H. Enhanced Removal of Basic Brown1 Dye from Aqueous Solutions by Sawdust Activated Carbon. Equilibrium, Thermodynamic and Kinetics. *Desalin. Water Treat.* **2024**, *317*, 100057. [[CrossRef](#)]
55. Zhang, T.; Zhang, X.; Li, H. Kinetics and Equilibrium Study of Phenol Adsorption by Activated Carbon Derived from Pig Blood. *Carbon Trends* **2023**, *12*, 100281. [[CrossRef](#)]
56. Cao, S.; Zhu, R.; Wu, D.; Su, H.; Liu, Z.; Chen, Z. How hydrogen bonding and π – π interactions synergistically facilitate mephedrone adsorption by bio-sorbent: An in-depth microscopic scale interpretation. *Environ. Pollut.* **2024**, *342*, 123044. [[CrossRef](#)] [[PubMed](#)]
57. Khumalo, S.M.; Bakare, B.F.; Rathilal, S. Single and Multicomponent Adsorption of Amoxicillin, Ciprofloxacin, and Sulfamethoxazole on Chitosan-Carbon Nanotubes Hydrogel Beads from Aqueous Solutions: Kinetics, Isotherms, and Thermodynamic Parameters. *J. Hazard. Mater. Adv.* **2024**, *13*, 100404. [[CrossRef](#)]
58. Hisana; Shahzaib, A.; Nishat, N.; Alshehri, S.M.; Ahamad, T.; Haque, Z. Biogenically Fabricated Tulsi-Infused ZnO–CuO Nanocomposites for Enhanced Dye Reduction and Adsorption. *Hybrid Adv.* **2024**, *5*, 100145. [[CrossRef](#)]
59. Aguilar, M.I.; Lloréns, M.; Ortuño, J.F.; Meseguer, V.F.; Pérez-Marín, A.B.; Cases, A. Use of the Box–Behnken Experimental Design for the Optimization of Orange II (Acid Orange 7) Adsorption on Aloe Vera. *Sustainability* **2023**, *15*, 15727. [[CrossRef](#)]
60. Chaudhuri, M.; Zaid, N.A.M.; Elmolla, E.S. Coconut Coir Activated Carbon: An Adsorbent for Removal of Textile Acid Azo Dye from Aqueous Solution. In Proceedings of the 2012 IEEE Colloquium on Humanities, Science and Engineering (CHUSER), Kota Kinabalu, Malaysia, 3–4 December 2012; IEEE: Piscataway, NJ, USA, 2012; pp. 58–62. [[CrossRef](#)]
61. El-Nemr, M.A.; El Nemr, A.; Hassaan, M.A.; Ragab, S.; Tedone, L.; De Mastro, G.; Pantaleo, A. Microporous Activated Carbon from Pisum Sativum Pods Using Various Activation Methods and Tested for Adsorption of Acid Orange 7 Dye from Water. *Molecules* **2022**, *27*, 4840. [[CrossRef](#)]
62. Silva, J.P.; Sousa, S.; Rodrigues, J.; Antunes, H.; Porter, J.J.; Gonçalves, I.; Ferreira-Dias, S. Adsorption of acid orange 7 dye in aqueous solutions by spent brewery grains. *Sep. Purif. Technol.* **2004**, *40*, 309–315. [[CrossRef](#)]
63. Supriya, S.; Palanisamy, P.N. Adsorptive removal of acid orange 7 from industrial effluents using activated carbon and conducting polymer composite—A comparative study. *Indian J. Chem. Technol.* **2016**, *23*, 506–512. [[CrossRef](#)]

Disclaimer/Publisher’s Note: The statements, opinions and data contained in all publications are solely those of the individual author(s) and contributor(s) and not of MDPI and/or the editor(s). MDPI and/or the editor(s) disclaim responsibility for any injury to people or property resulting from any ideas, methods, instructions or products referred to in the content.